TURBULENT MIXING IN A PRECESSING SPHERE

Susumu Goto
Graduate School of Engineering Science, Osaka University,
1-3 Machikaneyama, Toyonaka, Osaka, 560-8531 Japan
goto@me.es.osaka-u.ac.jp

Masaki Shimizu and Genta Kawahara
Graduate School of Engineering Science, Osaka University,
1-3 Machikaneyama, Toyonaka, Osaka, 560-8531 Japan

ABSTRACT

Strong turbulence is sustained in a precessing smooth cavity. Since industrial applications of this system to mixer, chemical reaction chamber, etc. are expected, we quantify the mixing ability of sustained turbulence in a precessing sphere by the help of direct numerical simulations. More concretely, fluid particles in the sphere are numerically tracked, and the time for initially separated particles by a central plane to be mixed is evaluated. Statistics of turbulence in the sphere depend strongly on the rate of precession (the Poincaré number), and therefore the mixing ability is also controlled by this parameter. When the Reynolds number defined by the spin angular velocity, the radius of sphere and the kinematic viscosity of fluid is fixed at $Re = 40000$, the most efficient mixing is achieved when Poincaré number is about 0.07.

Introduction

In this paper, we propose an effective technique to mix the confined fluid in a smooth cavity only by its rotational motion. Recall that, in general, fluid motion in a cavity rotating at a constant angular velocity always settles down to the solid-body rotational flow. This fact implies that an unsteady rotation of vessel is necessary to sustain efficient mixing of confined fluid.

In the following, we shed light on one of the simplest unsteady rotational motions of a cavity: i.e. the so-called precession. A precession is the rotation of spin axis around another axis (the precession axis); see an example of a precessing sphere in figure 1. In the following, we restrict ourselves in the case that the two axes are orthogonal. Although it is well-known mainly by geophysicists (the spin axis of the Earth is precessing weakly) since the seminal experiment by Malkus (1968) that a weak precession of a cavity can lead to developed turbulence of the confined fluid (see also experiments by Vanyo 1973, 1991; Manasseh 1992, 1994, 1996; Kobine 1995, 1996; Vanyo *et al.* 1995; Vanyo & Dunn 2000; Noir *et al.* 2001*b*,*a*, 2003; Cardin & Olson 2007; Meunier *et al.* 2008; Lagrange *et al.* 2008 and numerical studies by Hollerbach & Kerswell 1995; Tilgner 1999*a*,*b*; Tilgner & Busse 2001; Lorenzani & Tilgner 2001, 2003; Tilgner 2005, 2007; Wu & Roberts 2009; Nore & Leorat 2011; Koike *et al.* 2012), its engineering application is quite limited.

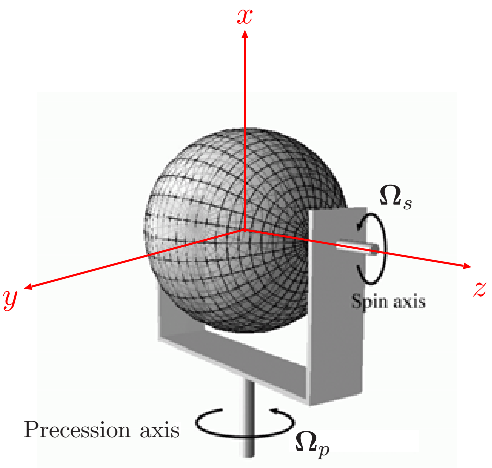

Figure 1. Precessing sphere. The spin and the precession axes are set to be orthogonal. The coordinate (x,y,z) is fixed in the precession frame, which rotates at a constant angular velocity $\boldsymbol{\Omega}_p$.

As shown in our previous experiments (Goto *et al.*, 2007, 2011), this system is likely to have wide applications as an efficient mixer without impellers. So this paper aims at evaluating, by direct numerical simulations (DNS), the mixing efficiency of turbulence sustained in the precessing sphere (figure 1).

Direct Numerical Simulations

One of the advantages of this system is that we can conduct DNS under the precisely same condition as in laboratory experiments. Since DNS are more suitable for quantitative evaluation of mixing efficiency than experiments, we perform DNS of turbulence in a precessing sphere by solving the Navier-Stokes equations

$$\frac{\partial}{\partial t}\boldsymbol{u}+\boldsymbol{u}\cdot\nabla\boldsymbol{u}=-\nabla p+\frac{1}{Re}\nabla^2\boldsymbol{u}+2\Gamma\,\boldsymbol{u}\times\widehat{\boldsymbol{e}}_p \qquad (1)$$

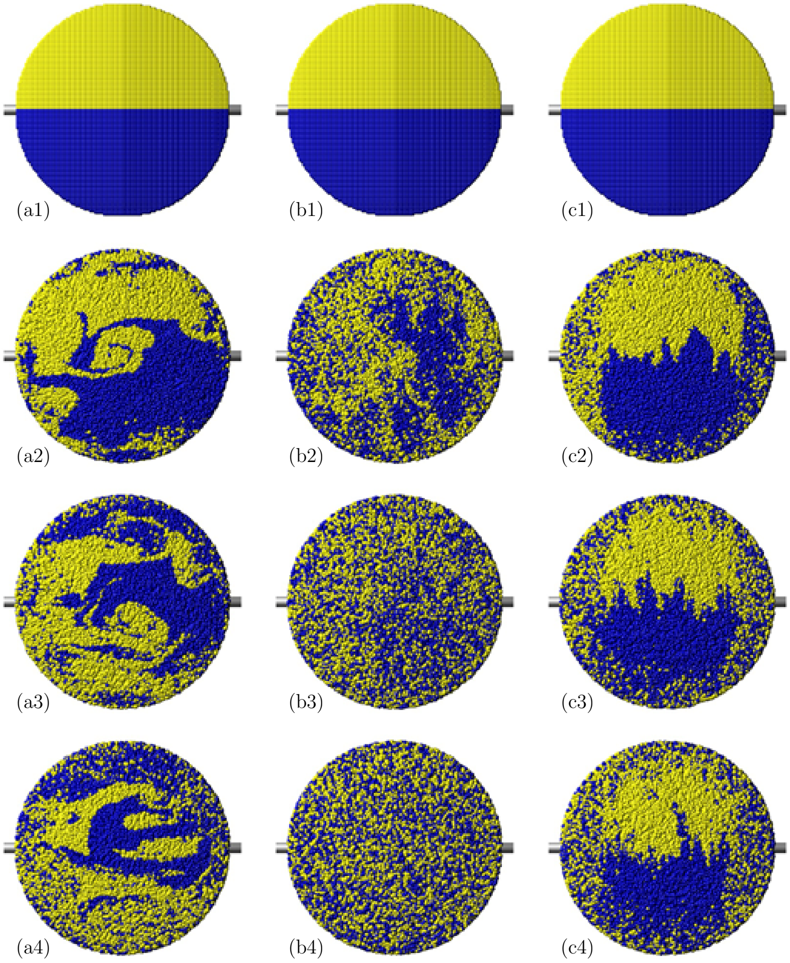

Figure 2. Temporal evolution of mixing of two fluids. Fluid particles in a thin layer $|y| < 0.05a$ are visualized. Their color (blue or yellow) is determined at the initial time. $Re = 40000$. (a) $\Gamma = 0.01$, (b) 0.1 and (c) 0.4. (1) $\widehat{t} = 0$, (2) $5T_s$, (3) $10T_s$ and (4) $15T_s$.

and the continuity equation

$$\nabla \cdot \boldsymbol{u} = 0 \tag{2}$$

for an incompressible fluid under the non-slip boundary condition

$$\boldsymbol{u} = \widehat{\boldsymbol{e}}_s \times \boldsymbol{r} \, . \tag{3}$$

on the spherical wall. In the above governing equations in a non-dimensional form, $\boldsymbol{u}(\boldsymbol{r},t)$, $p(\boldsymbol{r},t)$, $\boldsymbol{r}$ and t are non-dimensionalized velocity field, pressure field, position vector and time, respectively; where the radius a of the sphere and the reciprocal ${\Omega_s}^{-1}$ of the magnitude of spin angular velocity are employed as characteristic length and time. $\boldsymbol{e}_s$ and $\boldsymbol{e}_p$ denote the unit vectors parallel to the spin and the precession axes, respectively.

Note that since (1)–(3) depend only on the two non-dimensional parameters,

$$Re = \frac{a^2 \Omega_s}{\nu} \quad \text{(Reynolds number)}\,, \tag{4}$$

where ν is the kinematic viscosity of fluid, and

$$\Gamma = \frac{\Omega_p}{\Omega_s} \quad \text{(Precession rate, Poincaré number)}\,; \tag{5}$$

these two parameters Re and Γ control the system.

In our DNS, in order that (2) is precisely satisfied, the velocity field is expressed by two scalar fields as

$$\boldsymbol{u} = \nabla \times \big(\nabla \times (\boldsymbol{r}\Phi)\big) + \nabla \times (\boldsymbol{r}\Psi)\,, \tag{6}$$

and the governing equations for these two scalar fields ($\Phi(\boldsymbol{r},t)$ and $\Psi(\boldsymbol{r},t)$) are numerically solved. The spatial derivatives in the governing equations are estimated by the spectral method (where the spherical harmonics and the Zernike spherical polynomials are employed; see Kida & Shimizu (2011) for more details); whereas the temporal integration is made by the second-order Adams-Bashforth method and the Crank-Nicolson method. It has been verified that statistics (such as the mean velocity and turbulence intensity) of simulated turbulence precisely coincide with the result of our particle image velocimetry in the laboratory.

In order to estimate mixing efficiency, we track I fluid particles advected by the simulated turbulence. These particles are distributed uniformly in the sphere at a time ($\widehat{t} = 0$) when turbulence is in a statistically stationary state. The position vector $\boldsymbol{x}_i$ of the i-th particle is simulated by integrating the advection equation,

$$\frac{\mathrm{d}\boldsymbol{x}_i}{\mathrm{d}t} = \boldsymbol{u}\big(\boldsymbol{x}_i(t), t\big)\,, \tag{7}$$

by the second-order Adams-Bashforth method.

Examples of thus simulated particle distributions are shown in figure 2 for three different Poincaré numbers $\Gamma = 0.01$, 0.1 and 0.4 at a fixed Reynolds number $Re = 40000$. Only the fluid particles in a thin central layer of the sphere are shown in this figure. T_s denotes the period of spin.

Mixing Efficiency Estimation

Mixing efficiency is estimated as follows. First, we divide the fluid particles into two groups (say, group-A and -B) at the initial time ($\widehat{t} = 0$) of particle tracking; e.g. the blue and yellow particles in figure 2. Secondly, we divide the spherical cavity into J sub-domains of same volume δV, and let ρ_j be $n_{Aj}/(n_{Aj} + n_{Bj})$ where n_{Aj} and n_{Bj} are the numbers of particles of A- and B-group, respectively, in the j-th sub-domain. Then, the mixing index $\mathscr{M}$ is defined by

$$\mathscr{M} = 1 - 2\sigma \qquad \text{(mixing index)} \tag{8}$$

where $\sigma = \sqrt{\frac{1}{J}\sum_{j=1}^{J}(\rho_j - 0.5)^2}$ is the standard deviation of ρ_j.

Note that (i) when the particles are perfectly segregated (i.e. ρ_j takes the value either 0 or 1), $\mathscr{M} = 0$ because $\sigma = 0.5$; and that (ii) when the mixing is completed (i.e. ρ_j becomes 0.5 in all the sub-domains), $\mathscr{M} = 1$ because σ becomes zero. (For simplicity, we have assumed that the number of particles in group-A is the same as that in group-B.)

This mixing index was originally proposed by Danckwerts (1952) and has been used in the field of chemical engineering. In practice, however, we may track only a finite number of particles, then the standard deviation σ of ρ_j does not vanish and takes a finite value of $\widetilde{\sigma} = \sqrt{J/4I}$ even when the mixing is completed. We have assumed, in the derivation of the above expression of $\widetilde{\sigma}$, that I/J is not too small. Note also that $\widetilde{\sigma} \to 0$ as $I/J \to \infty$. Therefore, in our DNS with a finite number of particles, the mixing index (8) should better to be modified as

$$\widetilde{\mathscr{M}} = \frac{1 - 2\sigma}{1 - 2\widetilde{\sigma}} \qquad \text{(modified mixing index)} \tag{9}$$

so that $\widetilde{\mathscr{M}}$ becomes 1 for the perfect mixing.

Results

Our laboratory experiments show that large-scale motions of turbulence at sufficiently high Re are independent of Re and determined only by the Poincaré number Γ. This remarkable observation is verified also by our DNS (Koike *et al.*, 2012). These observations imply that the mixing efficiency is also controlled mainly by the Poincaré number Γ. Therefore, here we report DNS results for different Poincaré numbers Γ at a fixed Reynolds number $Re = 40000$.

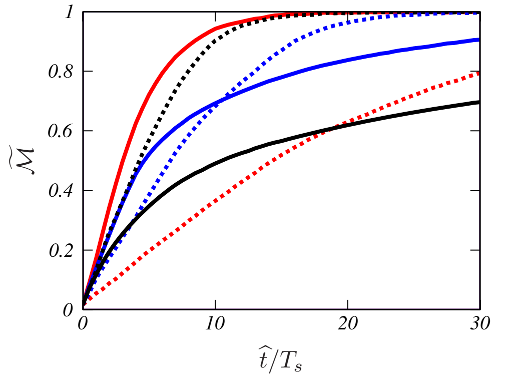

Figure 3. Temporal evolution of the mixing index $\widetilde{\mathscr{M}}$ defined by (9) for the sub-domain size $\delta V/a^3 \approx 2.5 \times 10^{-4}$. Reynolds number is fixed at $Re = 40000$. Poincaré number $\Gamma = 0.01$, - - - - -; 0.02, - - - - -; 0.04, - - - - -; 0.1, ——; 0.2, ——; 0.4, ——.

A main result is shown in figure 3, where the temporal evolution of the modified mixing index $\widetilde{\mathscr{M}}$ is plotted for different Γ. It is clearly observed in this figure that the mixing efficiency depends strongly on the Poincaré number Γ, and the most efficient mixing takes place when Γ is between 0.04 and 0.1.

This result is consistent with the experimental observation. Flow visualizations by reflective flakes are shown in figure 4 for the same Reynolds number ($Re = 40000$) as in the present DNS. Turbulence is quiescent for smaller (figure 4a) or larger (c) Poincaré numbers because the rotation of vessel around the spin axis or the precession axis dominates and turbulence tends to simple rotational flow around each axis. For example, in the larger Γ case, laminar structure along the precession axis is observed in the central region of the sphere (figure 4c); this is consistent with the DNS result (figure 2c) that the turbulent mixing is rather weak in the region. When the Poincaré number Γ is around 0.1, on the contrary, large-scale internal shear flow is created in the central region of sphere, and developed turbulence with fine structures (figure 4b) is sustained inside the sphere. This is the reason why strong mixing takes place for this parameter.

As a further detailed analysis, we have evaluated $\widetilde{\mathscr{M}}$ at $\widehat{t} = 10T_s$ (where T_s denotes spin period) for the Poincaré numbers between $\Gamma = 0.04$ and 0.1. Then, it is shown that the most efficient mixing takes place when $\Gamma \approx 0.07$ and $\widetilde{\mathscr{M}}(10T_s) \approx 0.98$ for this Γ. This result implies that the mixing is completed after only 10 spin periods for this relatively small Poincaré number, $\Gamma = 0.07$.

Conclusion

Conducting DNS of turbulence in a precessing sphere and of fluid particles advected by the turbulence, the efficiency of turbulent mixing is evaluated. As an example, the mixing of two fluids initially separated by the central plane perpendicular to the precession axis is investigated. It is then shown that mixing is most efficient when the Poincaré number (5) is very small ($\Gamma \approx 0.07$) for the fixed Reynolds number at $Re = 40000$, and that almost perfect mixing requires only 10 spin periods. This is consistent with our experimental observation (figure 4) that most developed turbulence is sustained in the sphere when $\Gamma = O(0.1)$ for a fixed Reynolds number. Physical mechanism of this effi-

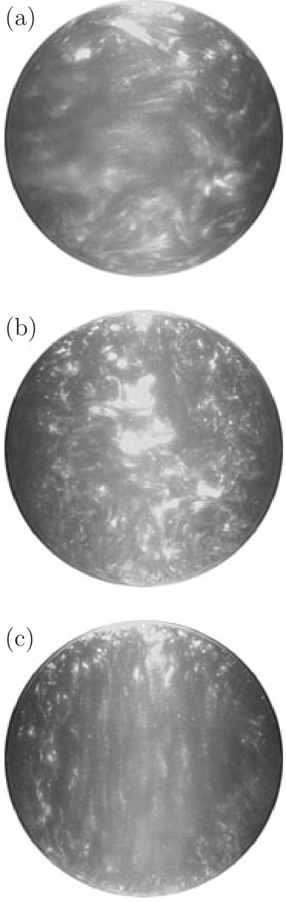

Figure 4. Turbulence sustained in the precessing sphere. Visualization by reflective flakes in the laboratory. $Re = 40000$. (a) $\Gamma = 0.01$, (b) 0.1 and (c) 0.4. The perspective is along the spin axis, and the vertical direction in the figure is parallel to the precession axis.

cient mixing in the weakly precessing sphere is under instigation on the basis of DNS data analysis.

This work was supported by JSPS KAKENHI Grant Numbers 24360071 and 24540416.

REFERENCES

Cardin, P. & Olson, P. 2007 Experiment on core dynamics. *Core dynamics of Treatise of Geophysics* **8**, 319–345.

Danckwerts, P. V. 1952 The definition and measurement of some characteristics of mixtures. *App. Sci. Res. A* **3**, 279–296.

Goto, S., Fujiwara, M. & Yamato, M. 2011 Turbulence sustained in a precessing sphere and spheroids. In *Proc. TSFP-7*.

Goto, S., Ishii, N., Kida, S. & Nishioka, M. 2007 Turbulence generator using a precessing sphere. *Phys. Fluids* **19**, 061705.

Hollerbach, R. & Kerswell, R. R. 1995 Oscillatory internal shear layers in rotating and precessing flows. *J. Fluid Mech.* **298**, 327–339.

Kida, S. & Shimizu, M. 2011 A turbulent ring and dynamo in a precessing sphere. *J. Phys.: Conf. Ser.* **318**, 072031.

Kobine, J. J. 1995 Inertial wave dynamics in a rotating and precessing cylinder. *J. Fluid Mech.* **303**, 233–252.

Kobine, J. J. 1996 Azimuthal flow associated with inertial wave resonance in a precessing cylinder. *J. Fluid Mech.* **319**, 387–406.

Koike, Y., Shimizu, M., Kida, S., Kawahara, G. & Goto, S. 2012 Continuous spin-up and dynamo in a precessing sphere. In *Proc. JSST 2012*.

Lagrange, R., Eloy, C., Nadal, F. & Meunier, P. 2008 Instability of a fluid inside a precessing cylinder. *Phys. Fluids* **65**, 081701.

Lorenzani, S. & Tilgner, A. 2001 Fluid instabilities in precessing spheroidal cavities. *J. Fluid Mech.* **447**.

Lorenzani, S. & Tilgner, A. 2003 Inertial instabilities of fluid flow in precessing spheroidal shells. *J. Fluid Mech.* **492**.

Malkus, W. V. R. 1968 Precession of the earth as the cause of geomagnetism. *Science* **160**, 259–264.

Manasseh, R. 1992 Breakdown regimes of inertia waves in a precessing cylinder. *J. Fluid Mech.* **243**, 261–296.

Manasseh, R. 1994 Distortions of inertia waves in a rotating fluid cylinder forced near its fundamental mode resonance. *J. Fluid Mech.* **265**, 345–370.

Manasseh, R. 1996 Nonlinear behaviour of contained inertia waves. *J. Fluid Mech.* **315**, 151–173.

Meunier, P., Eloy, C., Lagrange, R. & Nadal, F. 2008 A rotating fluid cylinder subject to weak precession. *J. Fluid Mech.* **599**, 405–440.

Noir, J., Brito, D., Aldridge, K. & Cardin, P. 2001*a* Experimental evidence of inertial waves in a precessing spheroidal cavity. *Geophy. Res. Lett.* **28**, 3785–3788.

Noir, J., Cardin, P., Jault, D. & Masson, J.-P. 2003 Experimental evidence of nonlinear resonance effects between retrograde precession and the tilt-over mode within a spheroid,. *Geophys. J. Int.* **154**, 407–416.

Noir, J., Jault, D. & Cardin, P. 2001*b* Numerical study of the motions within a slowly precessing sphere at low eckman number. *J. Fluid Mech.* **437**, 282–299.

Nore, C. & Leorat, J. 2011 Nonlinear dynamo action in a precessing cylindrical container. *Phys. Rev. E* **84**, 016317.

Tilgner, A. 1999*a* Magnetohydrodynamics flow in precessing spherical shells. *J. Fluid Mech.* **379**, 303–318.

Tilgner, A. 1999*b* Non-axisymmetric shear layers in precessing fluid ellipsoidal shells. *Geophys. J. Int.* **136**, 629–636.

Tilgner, A. 2005 Precession driven dynamos. *Phys. Fluids* **17**, 034104.

Tilgner, A. 2007 Kinematic dynamos with precession driven flow in a sphere. *Geophys. Astrophys. Fluid Dyn.* **101**, 1–9.

Tilgner, A. & Busse, F. H. 2001 Fluid flows in precessing spherical shells. *J. Fluid Mech.* **426**, 387–396.

Vanyo, J., Wilde, P., Cardin, P. & Olson, P. 1995 Experiments on precessing flows in the earth's liquid core. *Geophys. J. Int.* **121**, 136–142.

Vanyo, J. P. 1973 An energy assessment for liquids in filled precessing spherical cavity. *J. Appl. Mech.* **41**, 1128–1130.

Vanyo, J. P. 1991 A geodynamo powered by luni-solar precessione. *Geophys. Astrophys. Fluid dyn.* **59**, 209–234.

Vanyo, J. P. & Dunn, J. R. 2000 Core precession: flow structures and energy. *Geophys. J. Int.* **142**, 409–425.

Wu, C. C. & Roberts, P. H. 2009 On a dynamo driven by topographic precession. *Geophys. Astrophys. Fluid Dyn.* **103**, 467–501.